Chinese Journal of Aeronautics, (2015), 28(3): 845–852

Chinese Society of Aeronautics and Astronautics
& Beihang University

Chinese Journal of Aeronautics

cja@buaa.edu.cn
www.sciencedirect.com

Disturbance observer-based robust guidance for Mars atmospheric entry with input saturation

Yiyu Zheng, Hutao Cui *

Deep Space Exploration Research Center, Harbin Institute of Technology, Harbin 150001, China

Received 16 September 2014; revised 22 December 2014; accepted 24 March 2015
Available online 17 April 2015

KEYWORDS

Disturbance observer;
Guidance;
Input saturation;
Mars atmospheric entry;
Robustness

Abstract With low-lifting capability taken into account, a robust guidance law for Mars entry vehicles with low lift-to-drag ratios, such as Mars Science Laboratory (MSL), is presented. Consider the nonlinear term in the drag dynamic equation and bounded disturbances as a lumped disturbance, and design a linear disturbance observer (DOB) to estimate it. With the consideration of the control input saturation, an innovative sliding surface and a virtual system are introduced to design the guidance law. Analyses of disturbance observer performance and Lyapunov-based transient performance are also presented. It is shown that the drag tracking error can be adjustable by explicit choices of design parameters. Simulation results confirm the effectiveness of the proposed guidance law.

1. Introduction

On 5 August 2012, Mars Science Laboratory (MSL) successfully landed inside Gale Crater and became the seventh U.S. vehicle landing successfully on Mars. With the application of a hypersonic guidance, MSL successfully carried out a more accurate landing than previous spacecraft to Mars, such as Vikings I and II, MER Spirit and Opportunity, Pathfinder and Phoenix. The MSL mission finally delivered a nearly 900 kg rover to a final position approximately 2 km from the 4.5965 ° S and 137.4019 ° E target within an expected touchdown ellipse of 19.1 km × 6.9 km.[1] Also, MSL entry vehicle is the first Mars entry vehicle to perform a guided entry.

MSL entry guidance is divided into three distinct phases according to the order that they occur[2]: pre-bank, range control and heading alignment. Once the filtered drag acceleration magnitude exceeds 1.96 m/s^2 (0.2 Earth g), the MSL entry guidance ceases the pre-bank and begins the range control. During this phase, MSL entry vehicle adopts the entry terminal point controller (ETPC) which is derived from the Apollo final entry phase guidance algorithm[2–5] and modulates the bank angle to control the range flown. A three-segment bank profile is used to meet the parachute deployment constraints and generate a reference trajectory.[2] The time-varying controller gains of the ETPC are generated using influence coefficients with respect to errors about the reference trajectory stored by range-to-go, drag acceleration and altitude rate as a function of relative velocity.[6–9] Similar to the Apollo entry guidance, a bank-reversal logic is used to determine the sign of the bank angle. Whenever the cross range

* Corresponding author. Tel.: +86 451 86418320 312.
E-mail address: cuiht@hit.edu.cn (H. Cui).

Peer review under responsibility of Editorial Committee of CJA.

ELSEVIER Production and hosting by Elsevier

http://dx.doi.org/10.1016/j.cja.2015.04.014

to the target exceeds the dead band,[2] which is described as a quadratic function of velocity, the sign of the bank angle is changed to the opposite. Due to larger atmospheric density variations and shorter flight times, a tighter cross range corridor is added for the first bank reversal,[2,8] which improves the performance and reduces the cross range overshoot.

A Mars entry guidance task is to safely and accurately deliver an entry module from its initial conditions to a designated parachute deployment target at the end of the entry phase. To date, quite a few researchers have considered the problem of Mars entry guidance law design. It is universally acknowledged that Mars entry guidance can be divided into two categories[10]: predictive path-planning methods and reference-path tracking methods. Predictive path-planning methods rely on onboard computation for a real-time path planning and guidance solution, such as the predictive drag-based guidance law,[11] the numerical predictive-corrector guidance law[12,13] and analytical predictor–corrector guidance algorithms.[14,15] Reference-path tracking methods require not only a reference trajectory which is preplanned using nominal initial entry states and nominal dynamic models, but also a trajectory tracking control law. To address the problem of trajectory tracking control law design, some advanced control methods like the linear quadratic regulator method,[16,17] the feedback linearization method,[18,19] the state-dependent Riccati equation method,[20] the model reference adaptive control method,[21] active disturbance rejection control[22] and neural networks-based sliding mode variable structure control[23] etc., have been applied to the trajectory tracking control law design.

However, most studies mentioned above rarely take the low-lifting capability of a Mars entry module into account and assume the control input to work perfectly. It should be pointed out that lift-to-drag ratios are quite low and typically about 0.3 or even lower for Mars entry vehicles such as the MSL entry vehicle. These vehicles have a low-level control authority and limited maneuverability.[10,24] The control input is often subjected to saturation. Control input saturation often severely limits system performance, giving rise to undesirable inaccuracy or leading to instability.[25] Therefore, the design of a trajectory tracking controller with the consideration of control input saturation is an important issue and needs to be handled carefully. Another problem for the trajectory tracking controller design is the handling of large dispersions, mainly due to uncertainties of Martian atmosphere.

This paper develops a robust disturbance observer-based trajectory tracking controller for Mars entry vehicles with the control input saturation and the robustness problem taken into account. The nonlinear term and bounded disturbances in drag dynamics are regarded as a lumped disturbance. A linear disturbance observer, derived by the disturbance observer technology,[26–29] is employed to estimate the lumped disturbance. The estimate value is used as a feed-forward compensation to restrain the effects of the lumped disturbance on the trajectory tracking performance. With the difference between the control input and the saturated input as the input, a virtual system is constructed to compensate the effect of saturation. By introducing a novel sliding surface which relies on the drag tracking error and the virtual state, the disturbance observer-based trajectory tracking controller is finally obtained. It is shown that this controller is robust against the unknown bounded time-varying disturbance. Transient performance, which can be adjusted by tuning certain design parameters, is also analyzed in this paper.

2. Entry guidance problem formulation

For an unpowered atmospheric flight over the nonrotating, windless, spherical Mars and the longitudinal translational motion of the entry vehicle can be described by the downrange R, the radial distance form center of Mars r, the relative velocity V and the flight path angle γ as follows:[11]

$$\dot{r} = V\sin\gamma \tag{1}$$

$$\dot{V} = -D - g\sin\gamma \tag{2}$$

$$\dot{\gamma} = [L\cos\sigma - (g - V^2/r)\cos\gamma]/V \tag{3}$$

$$\dot{R} = V\cos\gamma \tag{4}$$

where σ is the bank angle, defined as the angle about the velocity vector from the local vertical plane to the lift vector; the gravitational acceleration g, the aerodynamic drag acceleration D and the lift acceleration L are given by

$$D = 0.5\rho V^2 S_{\text{ref}} C_D/m \tag{5}$$

$$L = 0.5\rho V^2 S_{\text{ref}} C_L/m \tag{6}$$

$$g = \mu/r^2 \tag{7}$$

where μ is the gravitational parameter; S_{ref} is the vehicle reference surface area; C_D and C_L are the aerodynamic drag and lift coefficients; ρ is the Mars atmospheric density; m is the mass of the vehicle. Assume an exponential atmospheric density model as

$$\rho = \rho_0 \exp((r_s - r)/h_s) \tag{8}$$

where ρ_0 is the density at the reference radius; r_s is the reference radius; h_s is the constant scale height.

Energy is used in place of time as the independent variable with the consideration that time is not critical in the entry flight. Define the energy as[13,21,22]

$$E = \frac{V^2}{2} - \frac{\mu}{r} \tag{9}$$

The derivative of E with respect to time is given by

$$\dot{E} = -DV < 0 \tag{10}$$

Therefore, the energy is a monotonically decreasing variable. Considering Eqs. (4) and (10), we obtain the derivate of downrange with respect to energy as

$$\frac{\mathrm{d}R}{\mathrm{d}E} = -\frac{\cos\gamma}{D} \tag{11}$$

Let's assume that the flight path angle is small in the entry flight. Then the downrange flown from the current energy E_0 to the final energy E_f can be approximated by Eq.(12):[10,11]

$$R = -\int_{E_0}^{E_f} \frac{\mathrm{d}E}{D} \tag{12}$$

It is clear that the downrange, as a function of the energy, depends mainly on the drag profile. The drag of an entry vehicle, in turn, can be controlled through the bank angle. If the drag profile is specified by a so-called reference drag profile D_r in advance and a drag tracking guidance law for bank angle magnitude modulation is employed to follow the reference drag profile ideally, then the downrange at the point where $E = E_f$ is also determined. In the guidance scheme of the range control phase, the outer loop predicts the downrange flown

using Eq. (12) and adjusts the reference drag profile D_r so that the predicted downrange flown equals the desired downrange. The inner loop modulates the bank angle so that the drag tracks the reference drag profile and that the vehicle achieves the desired downrange.

3. Drag-based trajectory tracking design for range control

In this section, the goal is to develop a novel guidance law, in the presence of control input saturation and disturbances, for the reference drag profile tracking and controlling the downrange. With the control input saturation taken into account, we firstly present the drag dynamic equations in an appropriate form that benefits the controller design and analysis. Then we develop the disturbance observer-base controller design method and discuss the transient performance analysis of the drag tracking error.

3.1. Drag dynamic equations with control input saturation

Considering Eqs. (1)–(3), we obtain the drag dynamic with time as an independent variable[11]

$$\ddot{D} = a(D,\dot{D};r,\gamma,V) + b(D,\dot{D};r,\gamma,V)u \tag{13}$$

where

$$\begin{cases} a(D,\dot{D};r,\gamma,V) \\ = -\dfrac{\dot{D}V\sin\gamma}{h_s} + \dfrac{D(D+g\sin\gamma)\sin\gamma}{h_s} \\ \quad + \dfrac{D\cos^2\gamma(g-V^2/r)}{h_s} + \dfrac{2\dot{D}(D+g\sin\gamma)}{V^2} \\ \quad -2\dfrac{D(D+g\sin\gamma)^2}{V^2} - 2\dfrac{D\dot{D}}{V} + 4\dfrac{Dg}{r}\sin^2\gamma \\ \quad +2\dfrac{Dg\cos^2\gamma(g-V^2/r)}{V^2} \\ b(D,\dot{D};r,\gamma,V) = -D^2\left(\dfrac{2g}{V^2}+\dfrac{1}{h_s}\right)\dfrac{L}{D}\cos\gamma \end{cases}$$

$u = \cos\sigma$ is the control input.

The first derivative of drag with respect to time is

$$\dot{D} = \frac{-DV\sin\gamma}{h_s} - \frac{2D(D+g\sin\gamma)}{V} \tag{14}$$

Due to the cosine of the bank angle, the control input u should subject to saturation described by

$$\|u\| \leqslant 1 \tag{15}$$

where $\|\bullet\|$ is the 2-norm of a vector or scalar.

For the development of the guidance law with the consideration of the control input saturation, let's define a saturation function as

$$\mathrm{sat}(v) = \begin{cases} 1 & v \geqslant 1 \\ v & -1 < v < 1 \\ -1 & v \leqslant -1 \end{cases} \tag{16}$$

If we treat the nonlinear term $a(D,\dot{D};r,\gamma,V)$ and disturbances caused by parameter perturbation as a lumped disturbance d, then the actual drag dynamic equation with the control input saturation can be represented by the system

$$\ddot{D} = d + b_n\mathrm{sat}(v) \tag{17}$$

where b_n is the nominal value of $b(D,\dot{D};r,\gamma,V)$.

Observe that the control input $\mathrm{sat}(v) \in [-1,1]$, as a function of v, depends only on the new control input v. The drag tracking problem turns to find such a guidance law $v(t)$ that the vehicle drag follows the reference drag profile provided by the outer loop of the entry guidance scheme. By using this modeling approach, we transform the control input u which is limited between –1 and 1 to an unconstrained control input v. As shown later, this control input transformation simplifies the design of a controller and the analysis of drag tracking performance.

3.2. Disturbance observer-based controller design

Following Ref.[25], we define the difference between the control input v and the saturated input $\mathrm{sat}(v)$ as

$$\delta = \mathrm{sat}(v) - v \tag{18}$$

To compensate the effect of the saturation nonlinearity, we construct a virtual system as

$$\dot{\zeta} = -c_0\zeta + b_n\delta \tag{19}$$

with the initial condition that $\zeta(0) = 0$. In the constructed system, ζ is a virtual state and c_0 is a positive constant.The drag tracking error is defined as

$$e = D - D_r \tag{20}$$

where D_r is the reference drag profile. Choose a three-segment bank profile[2] to determine a trajectory via open-loop simulation using nominal models. The drag profile for this trajectory is taken as the reference drag profile.

The derivatives of the drag tracking error along the dynamics Eqs. (13) and (14) are

$$\dot{e} = \dot{D} - \dot{D}_r \tag{21}$$

$$\ddot{e} = d + b_n\mathrm{sat}(v) - \ddot{D}_r \tag{22}$$

Design an innovative sliding surface

$$s(e,\dot{e},\zeta) = \dot{e} + k_e e - \zeta \tag{23}$$

where k_e is a positive constant. It can be seen that the sliding surface not only relies on the drag tracking error but also the virtual state. The virtual state in the sliding surface here is expected to compensate the effect of the saturation nonlinearity. Differentiating the sliding surface with respect to time along the dynamics Eqs. (18), (21) and (22) yields

$$\dot{s} = d - \ddot{D}_r + k_e\dot{e} + b_n v + c_0\zeta \tag{24}$$

To design a linear disturbance observer for the lumped disturbance, we firstly transform the nonlinear system Eq. (24) to a linear system using a feedback linearization controller with the dynamic inverse technique:

$$v = (\ddot{D}_r - k_e\dot{e} - c_0\zeta + v_{fb})/b_n \tag{25}$$

where v_{fb} is a control that will be designed later. Substituting Eq. (25) into Eq. (24), we obtain a linear system with a persistent disturbance

$$\dot{s} = d + v_{fb} \tag{26}$$

Neglecting the lumped disturbance d in system Eq. (26), one has the nominal transfer function of the system Eq. (26) as $G_n(p) = 1/p$, with $p = \mathrm{d}(\bullet)/\mathrm{d}t$ denoting the differential

operator in this paper. Using the disturbance observer technology, we design the control v_{fb} as shown in Eq. (27) and the linear disturbance observer (DOB) for the lumped disturbance d as shown in Fig. 1.

$$v_{\mathrm{fb}} = -\hat{d} - k_{\mathrm{s}}s - 2\hat{\eta}s/(\|s\| + c_{\mathrm{s}}) \tag{27}$$

where $\hat{d}$ is the estimate value for d;c_{s} and k_{s} are both positive constants; $\hat{\eta}$ is an adaptive parameter with the dynamic:

$$\dot{\hat{\eta}} = l\|s\| \tag{28}$$

where l is a positive constant.

In Fig. 1, the Q-filter and ξ are respectively given by $Q(p) = 1/(\tau p + 1)$ and $\xi = -k_{\mathrm{s}}s - 2\hat{\eta}s/(\|s\| + c_{\mathrm{s}})$, with τ the time constant of the Q-filter. According to the disturbance observer technology, a small enough time constant τ is required to estimate the lumped disturbance with a sufficient precision. The time constant of the Q-filter in the linear DOB is generally selected as a compromised value to satisfy the dynamics and stability of the closed-loop control system. The general form and selection of binomial filters for the Q-filter have been suggested in Ref.[30].

Finally, we get the control law

$$v = [\ddot{D}_{\mathrm{r}} - k_{\mathrm{e}}\dot{e} - c_0\zeta - \hat{d} - k_{\mathrm{s}}s - 2\hat{\eta}s/(\|s\| + c_{\mathrm{s}})]/b_{\mathrm{n}} \tag{29}$$

With this controller and the saturation function defined in Eq. (16), we can calculate the disturbance observer-based control law u for reference drag profile tracking now.

4. Tracking performance of reference drag

In this section, we analyze the disturbance observer's performance and the transient performance of the drag tracking error. As shown later, if the lumped disturbance d is bounded and the time constant of the Q-filter is tuned to ensure that the steady-state gain of $Q(p)$ is 1, then the lumped disturbance can be asymptotically followed by the output of the linear DOB. From the transient performance analysis of the drag tracking error, we know that even the lumped disturbance can't be efficiently estimated by the linear DOB, and the steady drag tracking performance can be ensured and improved by tuning certain design parameters.

4.1. Disturbance observer performance analysis

From the block diagram of the system with the disturbance observer shown in Fig. 1, we obtain the transfer function of the estimation as

$$\hat{d}(p) = G_{\xi\hat{d}}(p)\xi(p) + G_{d\hat{d}}(p)d(p) \tag{30}$$

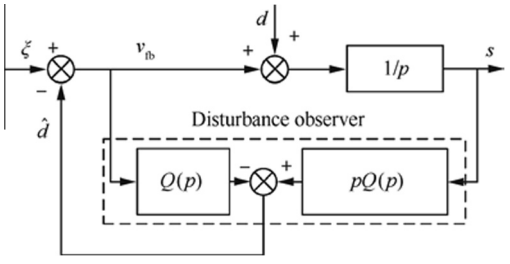

Fig. 1 Block diagram of system with disturbance observer.

where $G_{\xi\hat{d}}(p) = \hat{d}(p)/\xi(p) = 0$ and $G_{d\hat{d}}(p) = \hat{d}(p)/d(p) = Q(p)$. We define the estimation error for the lumped disturbance as

$$e_{\mathrm{d}}(p) = d(p) - \hat{d}(p) \tag{31}$$

Substituting Eq. (30) into Eq. (31) yields

$$e_{\mathrm{d}}(p) = (1 - Q(p))d(p) \tag{32}$$

It can be seen from Eq. (32) that the design of the DOB mainly depends on the design of the Q-filter. The Q-filter is usually designed to be a low-pass filter with a steady-state gain of 1 so that the estimate of the lumped disturbance approximately equals to the lumped disturbance and $Q(p)$ approaches to 1 in the domain of low-frequency. According to the final-value theorem, it can be further obtained that

$$\begin{aligned} e_{\mathrm{d}}(\infty) &= \lim_{p\to 0}(1 - Q(p))\lim_{p\to 0} pd(p) \\ &= d(\infty)\lim_{p\to 0}(1 - Q(p)) \end{aligned} \tag{33}$$

As shown in Fig. 1, the Q-filter of the linear DOB is selected as a first-order low-pass filter $Q(p) = 1/(\tau p + 1)$ with a steady-state gain of 1. We can tune the time constant of the Q-filter to achieve fine performance. As the lumped disturbance is bounded, we have $e_{\mathrm{d}}(\infty) = 0$. This implies that the lumped disturbance can be asymptotically followed by the output of the linear DOB. Note that the lumped disturbance includes the disturbances caused by parameter perturbations and the nonlinear term $a(D, \dot{D}; r, \gamma, V)$. They are both estimated by the linear DOB and feed-forward compensated by the output of the linear DOB. For the case when the steady-state gain of $Q(p)$ is not strictly 1, the DOB may not efficiently estimate the lumped disturbance. The estimation error may not be able to asymptotically reach the origin. Therefore, we need to consider the case when the linear DOB is only designed to ensure that the estimation error converges to a residual set defined as

$$\Lambda_1 = \{e_{\mathrm{d}} : \|e_{\mathrm{d}}\| \leqslant \eta_{\mathrm{e}}\} \tag{34}$$

where η_{e} is an unknown positive constant.

4.2. Convergence performance of drag tracking error

We firstly demonstrate that the boundary layer Λ_2 of Eq. (36) is an attractive invariant set for the sliding surface $s(e, \dot{e}, \zeta)$ and that $s(e, \dot{e}, \zeta)$ can be driven to arbitrarily small.

$$\Lambda_2 = \{s : \|s\| \leqslant c_{\mathrm{s}}\} \tag{35}$$

Let's define an estimate error for the unknown positive constant η_{e} in Eq. (34) as $\tilde{\eta} = \eta_{\mathrm{e}} - \hat{\eta}$, where $\hat{\eta}$ is the estimation of η_{e}. Taking the derivative of $\tilde{\eta}$ and using Eq. (28), one obtains

$$\dot{\tilde{\eta}} = -l\|s\| \tag{36}$$

The candidate of the Lyapunov function is chosen as

$$V_{\mathrm{s}} = 0.5s^2 + \frac{0.5\tilde{\eta}^2}{l} \tag{37}$$

Substituting Eq. (27) into Eq. (26), we have

$$\dot{s} = e_{\mathrm{d}} - k_{\mathrm{s}}s - \frac{2\hat{\eta}s}{\|s\| + c_{\mathrm{s}}} \tag{38}$$

For the case that $\|s\| > c_{\mathrm{s}}$, the derivative of V_{s} along the dynamics Eqs. (36) and (38) is

$$\begin{aligned}\dot{V}_s &= se_d - k_s s^2 - \frac{2\hat{\eta}s^2}{\|s\| + c_s} - \frac{\dot{\hat{\eta}}\tilde{\eta}}{l} \\ &\leqslant \|e_d\|\|s\| - k_s s^2 - \hat{\eta}\|s\| - \tilde{\eta}\|s\| \\ &\leqslant -k_s s^2 - \hat{\eta}\|s\| + \eta_e\|s\| - \tilde{\eta}\|s\| \\ &\leqslant -k_s s^2\end{aligned} \tag{39}$$

Thus, the Lyapunov function V_s and s are both bounded uniformly. The value of the Lyapunov function V_s keeps decreasing until $\|s\|$ is smaller than c_s. This indicates that Λ_2 is an attractive invariant set for s although the estimation error of the lumped disturbance is only able to converge to a residual set. By tuning parameter c_s, we can decrease s to a small value arbitrarily.

Let's consider the convergence performance of the drag tracking error. Define a positive Lyapunov function as

$$V_e = 0.5e^2 + 0.5\zeta^2 \tag{40}$$

The derivative of V_e along Eqs. (19) and (23) is

$$\begin{aligned}\dot{V}_e &= es - k_e e^2 + e\zeta + \zeta(-c_0\zeta + b_n\delta) \\ &\leqslant -(k_e - 2)e^2 + \zeta^2/2 + c_s^2/2 \\ &\quad -c_0\zeta^2 + b_n\zeta\delta \\ &\leqslant -(k_e - 2)e^2 + \zeta^2/2 + c_s^2/2 \\ &\quad -(c_0 - b_n^2/4)\zeta^2 + \delta^2\end{aligned} \tag{41}$$

If the parameters are chosen as

$$\begin{cases} c_0 = \dfrac{\bar{c}_0}{2} + \dfrac{b_n^2}{4} \\ k_e = 2 + \bar{k}_e \end{cases} \tag{42}$$

where $\bar{c}_0$ and $\bar{k}_e$ are both positive constants. Then, we have

$$\dot{V}_e \leqslant -\bar{k}_e e^2 + \frac{\zeta^2}{2} + \frac{c_s^2}{2} - 0.5\bar{c}_0\zeta^2 + \delta^2 \tag{43}$$

Integrating both sides of Eq. (43), one obtains

$$\begin{aligned}V_e(\infty) - V_e(0) \leqslant -\bar{k}_e \int_0^\infty \|e\|^2 \mathrm{d}t + 0.5\int_0^\infty \|c_s\|^2 \mathrm{d}t \\ +0.5(1 - \bar{c}_0)\int_0^\infty \|\zeta\|^2 \mathrm{d}t + \int_0^\infty \|\delta\|^2 \mathrm{d}t\end{aligned} \tag{44}$$

Thus

$$\begin{aligned}\|e\|_2^2 &= \int_0^\infty \|e\|^2 \mathrm{d}t \\ &\leqslant \tfrac{1}{k_e}\Big[-V_e(\infty) + V_e(0) + 0.5\int_0^\infty \|c_s\|^2 \mathrm{d}t \\ &\quad +0.5(1-\bar{c}_0)\int_0^\infty \|\zeta\|^2 \mathrm{d}t + \int_0^\infty \|\delta\|^2 \mathrm{d}t\Big] \\ &\leqslant \tfrac{V_e(0)}{k_e} + \tfrac{1}{k_e}\Big[0.5\int_0^\infty \|c_s\|^2 \mathrm{d}t \\ &\quad +0.5(1-\bar{c}_0)\int_0^\infty \|\zeta\|^2 \mathrm{d}t + \int_0^\infty \|\delta\|^2 \mathrm{d}t\Big]\end{aligned} \tag{45}$$

where $\|\bullet\|_2$ is the L_2-norm of a vector or scalar.

Construct a positive Lyapunov function $V_\zeta = 0.5\zeta^2$. The derivative of V_ζ along Eq. (19) is

$$\begin{aligned}\dot{V}_\zeta &= \zeta(-c_0\zeta + b_n\delta) = -c_0\zeta^2 + b_n\zeta\delta \\ &\leqslant -(c_0 - \tfrac{b_n^2}{4})\zeta^2 + \delta^2 \leqslant -0.5\bar{c}_0\zeta^2 + \delta^2\end{aligned} \tag{46}$$

Integrating both sides of Eq. (46), one obtains

$$V_\zeta(\infty) - V_\zeta(0) \leqslant -0.5\bar{c}_0\int_0^\infty \|\zeta\|^2 \mathrm{d}t + \int_0^\infty \|\delta\|^2 \mathrm{d}t \tag{47}$$

Considering the initial condition that $\zeta(0) = 0$, we have $V_\zeta(0) = 0$ and

$$\|\zeta\|_2^2 = \int_0^\infty \|\zeta\|^2 \mathrm{d}t \leqslant 2\|\delta\|_2^2/\bar{c}_0 \tag{48}$$

Substituting Eq. (48) into Eq. (45), we get

$$\|e\|_2^2 \leqslant \frac{V_e(0)}{\bar{k}_e} + \frac{\|c_s\|_2^2}{2\bar{k}_e} + \frac{\|\delta\|_2^2}{\bar{k}_e\bar{c}_0} \tag{49}$$

If the parameter satisfies $\bar{c}_0 \geqslant 2$, that is, $c_0 \geqslant 1 + b_n^2/4$, then

$$\|e\|_2^2 \leqslant \frac{V_e(0)}{\bar{k}_e} + \frac{\|c_s\|_2^2 + \|\delta\|_2^2}{2\bar{k}_e} \tag{50}$$

Considering $\bar{k}_e = (k_e - 2)$, we have

$$\|e\|_2^2 \leqslant \left(V_e(0) + \frac{\|c_s\|_2^2 + \|\delta\|_2^2}{2}\right) \Big/ (k_e - 2) \tag{51}$$

Thus, the drag tracking transient performance depends on parameters k_e and c_s as well as the initial drag tracking error $e(0)$ with the consideration that $V_e(0) = 0.5e^2(0)$. The smaller the initial drag tracking error is, the better the transient performance is. We can decrease the effects of the initial drag tracking error on the transient performance by increasing parameter k_e. Eq. (51) also shows that the transient performance can be improved by decreasing parameter c_s. The bound of $\|e\|_2$ depends on the bound of δ, the effects of which on the transient performance can be decreased by increasing parameter k_e. If $\delta \to 0$ as $t \to \infty$, then we have $\zeta \to 0$ and $e \to 0$.

5. Simulation and results

To illustrate the effectiveness of the proposed guidance law, a flight dynamics scenario simulating an MSL-class vehicle entering the Martian atmosphere is carried out in the MATLAB/Simulink environment. The guidance task is to deliver the vehicle to a terminal point where the velocity is 400 m/s and the altitude is not less than 7 km. After the vehicle reaches the entry interface, the bank angle is forced to be a constant pre-bank angle of 80°. If not, the initial cross-range may not be reduced efficiently and the dynamic pressure is also too low for the aerodynamic control to be effective. Once the drag acceleration magnitude exceeds 0.2 Earth g, the entry guidance ceases the pre-bank and begins the range control using the guidance law developed in this paper.

A three-segment bank profile[2] is used to generate the reference trajectory and the reference drag profile. During the range control phase, the magnitude of the commanded bank angle is not allowed to output a value greater than 90° or smaller than 30° in order to prevent a reduction of the cross-range control capability. When the velocity drops below 1100 m/s, the vehicle begins the heading alignment. The heading alignment logic is given as[2]

$$\sigma = K\arctan(R_c/R_{go}) \tag{52}$$

where $K = 2$ is the controller gain, R_c the cross-range and R_{go} the downrange to the target. To prevent the substantial loss of the parachute deploy altitude in this phase, the magnitude of the commanded bank angle is limited to 30° in the heading alignment phase. The schematic of the guidance architecture for this simulation is presented in Fig. 2.

A 500-run Monte Carlo simulation is carried out in this section to evaluate the effectiveness of the proposed guidance law. Detailed parameters of the entry vehicle come largely from the MSL-class mission data. They are given by:

$\mu = 4.283 \times 10^{13}$ m^3/s^2, $S_{ref} = 15.9$ m^2, $m = 3300$ kg, $C_D = 1.45$, $C_L = 0.348$, $r_s = 3394.5$ km, $\rho_0 = 0.0158$ kg/m^3 and $h_s = 9354$ km. The entry states and the corresponding errors are modeled as random Gaussian distributions at the entry interface that are listed in Table 1, where θ and ϕ are the longitude and latitude respectively of the position of the vehicle in spherical coordinates, and ψ is the heading angle of the velocity of the vehicle. The maximum density dispersion is specified as 20% in the Monte Carlo simulation, which is also modeled as a random Gaussian distribution. The parameters for the reference drag tracking guidance law developed in this paper are chosen as: $\tau = 0.1$, $c_s = 0.1$, $l = 0.01$, $k_s = 0.1$, $k_e = 2.1$ and $c_0 = 2 + b_n^2/4$. The simulation results are presented in Figs. 3–6.

Fig. 3 presents the reference bank angle and the reference drag profile obtained from the planning of the reference trajectory, as well as the actual drag and the absolute commanded bank angle computed from one of the Monte Carlo simulation. It can be seen from the absolute commanded bank angle shown in Fig. 3 that the range control nearly begins at 42 s and ends at 136 s. Although the actual bank angle magnitude is significantly different from the reference bank angle at the early range control phase, it remains mostly close to the reference value in this phase.

The drag tracking error and the sliding surface during the entry flight are shown in Fig. 4. The drag acceleration controlled by the proposed guidance law in this paper tracks the reference drag profile perfectly. The peak value of the drag tracking error is only smaller than 0.2 m/s^2. As expected, the peak value of the sliding surface is about 0.05, which is less than $c_s = 0.1$. This simulation result verifies that the boundary layer Λ_2 defined in Eq. (35) is an attractive invariant set for $s(e, \dot{e}, \zeta)$ with parameter $c_s = 0.1$. The three curves of the lumped disturbance, the disturbance estimate and the virtual state are presented in Fig. 5. The linear DOB is able to efficiently estimate the lumped disturbance during the drag tracking. The virtual state goes away from zero at 42 s and converges to the origin at about 75 s, which indicates that the control input saturation occurs at the early range control phase.

Fig. 6 presents the target miss distance for the 500-run Monte Carlo simulation at the parachute deployment, in which δ_c is the cross range error. Each small circle in Fig. 6 represents a single entry simulation. In this 500-run Monte Carlo simulation, 396 (or 79.2%) of the distances are within 3 km of the target and 98.2% are within 5 km of the target. The root mean square (RMS) of all the target miss distances

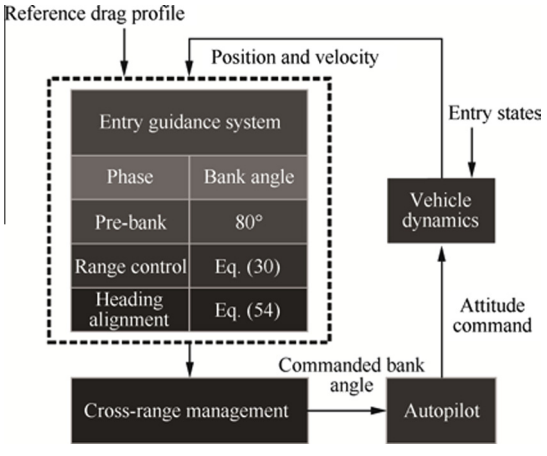

Fig. 2 Schematic of guidance architecture for Mars entry.

Table 1 Initial state dispersions.

Parameter	Initial value	Error (3σ)
r (km)	3522.02	0
θ (°)	0	0.1
φ (°)	0	0.01
V (m/s)	6000	5
γ (°)	−15	0.01
ψ (°)	0	0.01

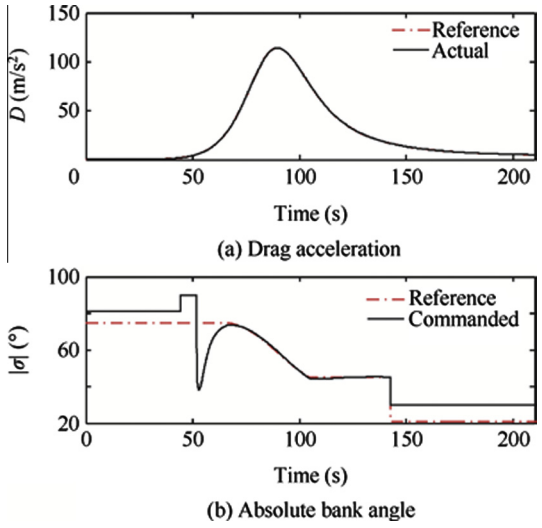

Fig. 3 Variation curves of absolute bank angle and drag acceleration.

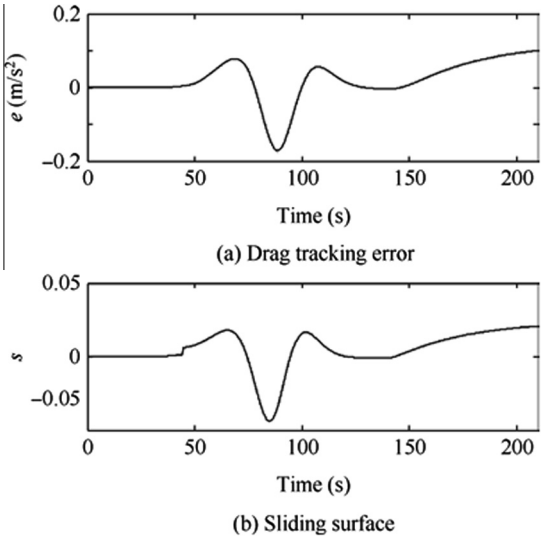

Fig. 4 Variation curves of drag tracking error and sliding surface.

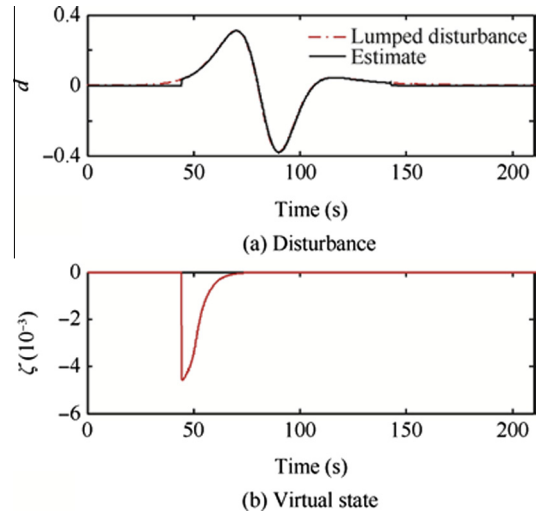

Fig. 5 Variation curves of disturbance and virtual state.

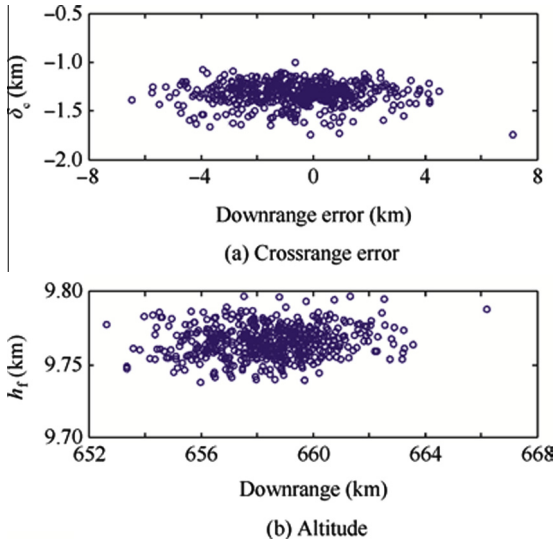

Fig. 6 Targeting errors and terminal altitude.

is 2.47 km. Fig. 6 also presents the histogram of the terminal altitude h_f at the parachute deployment. It can be seen that a majority of terminal altitudes are in the range between 9.7 km and 9.8 km.

6. Conclusions

In this paper, a linear disturbance observe-based guidance law for reference trajectory tracking has been developed for Mars atmospheric entry vehicles using a combination of the disturbance observer technique and sliding-model control. Disturbance observer performance analysis shows that the lumped disturbance can be asymptotically followed by the output of the linear DOB $\hat{d}$. With Lyapunov stability analysis and L_2 Gain-based stability analysis, the drag tracking transient performance is established and analyzed. It's shown that the transient performance can be improved with explicit tuning of design parameters.

The main contributions of this paper are as follows:

(1) A linear DOB is employed to estimate the lumped disturbance and is expected to restrain the effects of the lumped disturbance on the trajectory tracking performance.
(2) The linear DOB is only required to estimate the lumped disturbance with a bounded error, which helps reduce the difficulty of the DOB design.
(3) The guidance law developed in this paper is of robustness and continuity.
(4) The sliding surface in this paper not only relies on the drag tracking error but also the virtual state. This special design of the sliding surface allows us to design a guidance law with the control input saturation taken into account.

Acknowledgments

This work was co-supported by the National Basic Research Program of China (No. 2012CB720000) and the National Natural Science Foundation of China (No. 61174201).

References

1. Way DW, Davis JL, Shidner JD. Assessment of the Mars Science Laboratory entry, descent, and landing simulation. *Proceedings of the 23rd AAS/AIAA space flight mechanics meeting*; 2013 Feb 10–14; Kauai HI, USA. Washington, D.C: NASA; 2013. p. 563–81.
2. Mendeck GF, McGrew LC. Entry guidance design and postflight performance for 2011 Mars Science Laboratory mission. *J Spacecraft Rockets* 2014;**51**(3):1–12.
3. Mendeck G, McGrew L. Post-flight EDL entry guidance performance of the 2011 Mars Science Laboratory mission. *Proceedings of the 23rd AAS/AIAA space flight mechanics meeting*; 2013 Feb 10–14; Kauai HI, USA. Washington, D.C.: NASA; 2013. p. 547–62.
4. Brugarolis P, San MAM, Wong E. The entry controller for the Mars Science Laboratory. *Proceedings of the 23rd AAS/AIAA space flight mechanics meeting*; 2013 Feb 10–14; Kauai HI, USA. Washington, D.C.: NASA; 2013. p. 505–19.
5. Li S, Jiang X. Review and prospect of guidance and control for Mars atmospheric entry. *Prog Aerosp Sci* 2014;**69**:40–57.
6. Wingrove R. Survey of atmospheric re-entry guidance and control methods. *AIAA J* 1963;**1**(9):2019–29.
7. Carman G, Ives D, Geller D. Apollo-derived mars precision lander guidance. 1998. Report No.: AIAA-1998-4570.
8. Mendeck GF, Carman G. Guidance design for mars smart landers using the entry terminal point controller. 2002. Report No.: AIAA-2002-4502.
9. Coate RE, Lessing HC, Tunnell PJ. Lunar landing and long-range earth re-entry guidance by application of perturbation theory. *J Spacecraft Rockets* 1964;**1**(2):191–6.
10. Kluever CA. Entry guidance performance for Mars Science Laboratory landing. *J Guid Control Dynam* 2008;**31**(6):1537–44.
11. Tu KY, Munir MS, Mease KD, Bayard DS. Drag-based predictive tracking guidance for Mars precision landing. *J Guid Control Dynam* 2000;**23**(4):620–8.
12. Powell RW. Numerical roll reversal predictor corrector aerocapture and precision landing guidance algorithms for the Mars Surveyor Program 2001 missions. 1998. Report No.: AIAA-1998-4574.
13. Lu P. Entry guidance: a unified method. *J Guid Control Dynam* 2014;**37**(3):713–28.

14. Lafleur JM, Cerimele CJ. Angle of attack modulation for Mars entry terminal state optimization. *Proceedings of AIAA atmospheric flight mechanics conference*; 2009 Aug 10–13; Chicago, USA. Reston: AIAA; 2009. p. 1–20.
15. de Lafontaine J, Lévesque JF, Kron A. Robust guidance and control algorithms using constant flight path angle for precision landing on Mars. *Proceedings of AIAA guidance, navigation, and control conference*; 2006 Aug 21–24; Keystone, USA. Reston: AIAA; 2006. p. 583–603.
16. Roenneke AJ, Cornwell PJ. Trajectory control for a low-lift reentry vehicle. *J Guid Control Dynam* 1993;**16**(5):927–33.
17. Roenneke AJ, Cornwell PJ. Trajectory control for a low-lift maneuverable reentry vehicle. *Proceedings of aerospace design conference*; 1992 Feb 3–6; Ervin, USA. Reston: AIAA; 1992. p. 1–11.
18. Bharadwaj S, Rao AV, Mease KD. Entry trajectory tracking law via feedback linearization. *J Guid Control Dynam* 1998;**21**(5):726–32.
19. Mease KD, Kremer JP. Shuttle entry guidance revisited using nonlinear geometric methods. *J Guid Control Dynam* 1994;**17**(6):1350–6.
20. Steinfeldt BA, Tsiotras P. A state-dependent Riccati equation approach to atmospheric entry guidance. 2010. Report No.: AIAA-2010-8310.
21. Li S, Peng YM. Command generator tracker based direct model reference adaptive tracking guidance for Mars atmospheric entry. *Adv Space Res* 2012;**49**(1):49–63.
22. Xia YQ, Chen RF, Pu F, Dai L. Active disturbance rejection control for drag tracking in mars entry guidance. *Adv Space Res* 2014;**53**(5):853–61.
23. Li S, Peng YM. Neural networks based sliding mode variable structure control for Mars entry. *J Aerosp Eng* 2012;**226**(11):1373–86.
24. Meginnis IM, Putnam ZR, Clark IG, Brauns RD. Guided entry performance of low ballistic coefficient vehicles at Mars. *J Spacecraft Rockets* 2013;**50**(5):1047–59.
25. Zhou J, Wen C. *Adaptive backstepping control of uncertain systems*. London: Springer; 2008, p. 190–2.
26. Ohishi K, Nakao M, Ohnishi K. Microprocessor-controlled DC motor for load-insensitive position servo system. *IEEE Trans Ind Electron* 1987;**IE-34**(1):44–9.
27. Chu ZY, Sun FC, Cui J. Disturbance observer-based robust control of free-floating space manipulators. *IEEE Syst J* 2008;**2**(1):114–9.
28. Sun HB, Li SH. Composite control method for stabilizing spacecraft attitude in terms of Rodrigues parameters. *Chin J Aeronaut* 2013;**26**(3):687–96.
29. Zhang JP, Yan JJ, Li SH, Luo S. A guidance law design based on disturbance observer and backstepping. *Acta Aeronautica et Astronautica Sinica* 2012;**33**(12):2291–300 Chinese.
30. Umeno T, Hori Y. Robust speed control of DC servomotors using modern two degrees-of-freedom controller design. *IEEE Trans Industr Electron* 1991;**38**(5):363–8.

Zheng Yiyu received his B.S. degree in Mechanical Engineering from Xiamen University of Technology in 2011. He received his M.S. degree in Aerospace Engineering from Beijing Institute of Technology in 2014. He is currently working toward his Ph.D. degree in the Deep Space Exploration Research Center at Harbin Institute of Technology. His research interests include missile guidance and control, advanced Mars entry, descent and landing (EDL) technique, optimal control and nonlinear optimization.

Cui Hutao is a professor and Ph.D. advisor in the Deep Space Exploration Research Center at Harbin Institute of Technology. His current research interests focus on spacecraft guidance, navigation and control (GNC), especially on autonomous GNC for deep space missions.